ARMY RESEARCH LABORATORY

On the Shock Stress, Substructure Evolution, and Spall Response of Commercially Pure 1100-O Aluminum

by CL Williams, CQ Chen, KT Ramesh, and DP Dandekar

ARL-RP-0516 **December 2014**

A reprint from the Materials Science & Engineering A. 2014;618:596–604.

Approved for public release; distribution is unlimited.

NOTICES

Disclaimers

The findings in this report are not to be construed as an official Department of the Army position unless so designated by other authorized documents.

Citation of manufacturer's or trade names does not constitute an official endorsement or approval of the use thereof.

Destroy this report when it is no longer needed. Do not return it to the originator.

Army Research Laboratory
Aberdeen Proving Ground, MD 21005-5069

ARL-RP-0516 **December 2014**

On the Shock Stress, Substructure Evolution, and Spall Response of Commercially Pure 1100-O Aluminum

CL Williams and DP Dandekar
Weapons and Materials Research Directorate, ARL

CQ Chen and KT Ramesh
The Johns Hopkins University
Baltimore, MD

A reprint from the Materials Science & Engineering A. 2014;618:596–604.

Approved for public release; distribution is unlimited.

REPORT DOCUMENTATION PAGE

Form Approved
OMB No. 0704-0188

Public reporting burden for this collection of information is estimated to average 1 hour per response, including the time for reviewing instructions, searching existing data sources, gathering and maintaining the data needed, and completing and reviewing the collection information. Send comments regarding this burden estimate or any other aspect of this collection of information, including suggestions for reducing the burden, to Department of Defense, Washington Headquarters Services, Directorate for Information Operations and Reports (0704-0188), 1215 Jefferson Davis Highway, Suite 1204, Arlington, VA 22202-4302. Respondents should be aware that notwithstanding any other provision of law, no person shall be subject to any penalty for failing to comply with a collection of information if it does not display a currently valid OMB control number.
PLEASE DO NOT RETURN YOUR FORM TO THE ABOVE ADDRESS.

1. REPORT DATE *(DD-MM-YYYY)*	2. REPORT TYPE	3. DATES COVERED (From - To)
December 2014	Reprint	14 August 2012–9 November 2013

4. TITLE AND SUBTITLE
On the Shock Stress, Substructure Evolution, and Spall Response of Commercially Pure 1100-O Aluminum

5a. CONTRACT NUMBER

5b. GRANT NUMBER

5c. PROGRAM ELEMENT NUMBER

6. AUTHOR(S)
CL Williams, CQ Chen, KT Ramesh, and DP Dandekar

5d. PROJECT NUMBER

5e. TASK NUMBER

5f. WORK UNIT NUMBER

7. PERFORMING ORGANIZATION NAME(S) AND ADDRESS(ES)
US Army Research Laboratory
ATTN: RDRL-WMP-B
Aberdeen Proving Ground, MD 21005-5069

8. PERFORMING ORGANIZATION REPORT NUMBER
ARL-RP-0516

9. SPONSORING/MONITORING AGENCY NAME(S) AND ADDRESS(ES)

10. SPONSOR/MONITOR'S ACRONYM(S)

11. SPONSOR/MONITOR'S REPORT NUMBER(S)

12. DISTRIBUTION/AVAILABILITY STATEMENT
Approved for public release; distribution is unlimited.

13. SUPPLEMENTARY NOTES
A reprint from the Materials Science & Engineering A. 2014;618:596–604.

14. ABSTRACT
Plate impact shock and spall recovery experiments were conducted to study the effects of peak shock stress on the substructure evolution and spall response of fully annealed 1100 aluminum. The substructure of the material evolves substantially with increase in peak shock stress ranging from 4 GPa to 9 GPa with dislocation debris uniformly distributed throughout the interior of the subgrain. Observations from substructure evolution in conjunction with spall failure results suggest that ductile fracture by void nucleation, growth, and coalescence was perhaps the dominant fracture mode for shock stresses up to approximately 8.3 GPa. Whereas, beyond 8.3 GPa the material softened possibly due to dislocation reorganization (dynamic recovery) and brittle intergranular fracture by decohesion with isolated pockets of nanovoids was perhaps the dominant fracture mode. The contributions of nanovoids to the dynamic recovery process, if any, were unresolved. Microhardness measurements show an increase in residual hardness throughout the shock stress range studied implying shock hardening up to approximately 8.3 GPa. This observation also suggests that thermal softening was not operative throughout the shock stress range studied. However, dynamic recovery was thermally influenced during shock loading.

15. SUBJECT TERMS
shock, spall, plate impact, recovery, dislocations, dynamic recovery, aluminum, fracture

16. SECURITY CLASSIFICATION OF:			17. LIMITATION OF ABSTRACT	18. NUMBER OF PAGES	19a. NAME OF RESPONSIBLE PERSON
a. REPORT	b. ABSTRACT	c. THIS PAGE			CL Williams
Unclassified	Unclassified	Unclassified	UU	14	19b. TELEPHONE NUMBER (*Include area code*) 410-278-8753

Standard Form 298 (Rev. 8/98)
Prescribed by ANSI Std. Z39.18

Materials Science & Engineering A 618 (2014) 596–604

Contents lists available at ScienceDirect

Materials Science & Engineering A

journal homepage: www.elsevier.com/locate/msea

On the shock stress, substructure evolution, and spall response of commercially pure 1100-O aluminum

C.L. Williams [a,*], C.Q. Chen [b], K.T. Ramesh [b], D.P. Dandekar [a]

[a] U.S. Army Research Laboratory, Aberdeen Proving Ground, MD 21005-5066, USA
[b] The Johns Hopkins University, Baltimore, MD 21218-2681, USA

ARTICLE INFO

Article history:
Received 1 July 2014
Received in revised form
3 September 2014
Accepted 5 September 2014
Available online 16 September 2014

Keywords:
Shock stress
Shock hardening
Dynamic recovery
Substructure
Evolution
Recovery

ABSTRACT

Plate impact shock and spall recovery experiments were conducted to study the effects of peak shock stress on the substructure evolution and spall response of fully annealed 1100 aluminum. The substructure of the material evolves substantially with increase in peak shock stress ranging from 4 GPa to 9 GPa with dislocation debris uniformly distributed throughout the interior of the subgrain. Observations from substructure evolution in conjunction with spall failure results suggest that ductile fracture by void nucleation, growth, and coalescence was perhaps the dominant fracture mode for shock stresses up to approximately 8.3 GPa. Whereas, beyond 8.3 GPa the material softened possibly due to dislocation reorganization (dynamic recovery) and brittle intergranular fracture by decohesion with isolated pockets of nanovoids was perhaps the dominant fracture mode. The contributions of nanovoids to the dynamic recovery process, if any, were unresolved. Microhardness measurements show an increase in residual hardness throughout the shock stress range studied implying shock hardening up to approximately 8.3 GPa. This observation also suggests that thermal softening was not operative throughout the shock stress range studied. However, dynamic recovery was thermally influenced during shock loading.

Published by Elsevier B.V.

1. Introduction

Aluminum alloys such as the 2xxx, 5xxx, and 7xxx series are widely used in applications undergoing high rates of deformation because of their light weight, relatively high strength, and effective impact resistance. Additionally, they offer some advantages over steel that are quite attractive to designers, including better corrosion resistance, superior low-temperature embrittlement, and low cost. High velocity impacts under favorable conditions will result in shock waves which may lead to failure through the dynamic process known as spallation [1]. This process may be strongly influenced by microstructural evolution during the initial shock compression. Therefore, an in-depth study of the microstructural evolution under shock loading is essential for understanding the spall response of aluminum and aluminum alloys.

Previous studies have shown that the substructure evolution can play a major role in the shock response of metals and metallic alloys [2–16]. During the shock compression of metals and metallic alloys, large numbers of lattice defects such as dislocations can be introduced in the material which can lead to strengthening effects such as hardening and therefore change the material behavior [2–5,7,10–12,15,17]. However, the hardening that can result from substructure evolution is not unbounded and can therefore saturate at some critical shock stress; thereafter, the material may even begin to soften with further increase in shock stress. This latter behavior is normally attributed to dynamic recovery and recrystallization [5], perhaps as a consequence of shock induced heating. These hardening and softening processes are important for understanding the spall failure of materials. On the other hand, shock compression can also increase the number of potential void nucleation sites such as vacancies and vacancy clusters [6]. An increase in potential void nucleation sites can accelerate the failure of the material under tensile loading during the spall process, resulting in a reduction of the spall strength. Thus the spallation of a material is dependent on several competing mechanisms including dislocation generation, dislocation annihilation, generation of potential void nucleation sites, and temperature rise as a consequence of the shock compression prior to the tensile unloading that leads to spall failure.

The spall strength has been shown to be a strong function of the shock stress in a number of aluminum and aluminum alloys [8,18–21]. For example, the shock induced hardness of 6061-T6 aluminum has been observed to increase with shock stress until it saturates at a shock stress of approximately 8.0 GPa and decreases thereafter [8],[18]. Similarly, Chen et al. [19] observed that the

* Corresponding author. Tel.: +1 410 278 8753.
E-mail addresses: cyril.l.williams.civ@mail.mil, cwill115@jhu.edu (C.L. Williams).

http://dx.doi.org/10.1016/j.msea.2014.09.030
0921-5093/Published by Elsevier B.V.

shock stress dependence of the pullback velocity (a direct measure of spall strength) of 1060 aluminum saturated at a shock stress of approximately 13.5 GPa and then decreased for higher shock stresses. Furthermore, spall experiments conducted recently by Williams et al. [20,21] on 1100-O aluminum revealed that the spall strength increased with shock stress until it saturated at approximately 8.3 GPa and then decrease for higher shock stresses. Williams et al. [20,21] hypothesized that this type of behavior was due to work softening. The result obtained by Williams et al. [20,21] is shown in Fig. 1. These studies motivated this work, which is intended to investigate and develop an understanding of the substructural evolution of 1100-O aluminum under shock loading using plate impact recovery experiments.

We begin by describing the fundamental properties of the material investigated. Next, the shock-release and shock-release-spall recovery plate impact experiments performed are described. The substructure evolution results are then presented and discussed in the context of previous work [20,21]. Finally, conclusions are drawn based on the plate impact and microstructural evolution results.

2. Material properties

All test samples in this study were fabricated from the same batch of 1100-O aluminum employed by Williams et al. [20,21]. The 1100 aluminum alloy is commercially pure and fully annealed (O-temper) with silicon, iron, and copper as major alloying elements. Listed in Table 1 is the complete elemental make up (in percent weight) of the alloy. The microstructure of the as-received 1100-O aluminum was previously characterized by Williams et al. [20,21] using the Electron Backscatter Diffraction (EBSD) technique to obtain information on grain size, distribution, and orientation (Fig. 2). The average grain size was estimated to be approximately 250 μm. Although the vast majority of the grains are defined by high angle grain boundaries (misorientation $>15^{\circ}$ and represented by red in the figure), there is some evidence of low angle grain boundaries (misorientation $<10^{\circ}$ and represented by yellow in the figure) in the grain structure. The grain orientation map and inverse pole figure are also shown in Fig. 2 (b) and (c) respectively. Fig. 2(b) suggests that the preferred orientation or crystallographic texture of the annealed 1100 aluminum is nearly random.

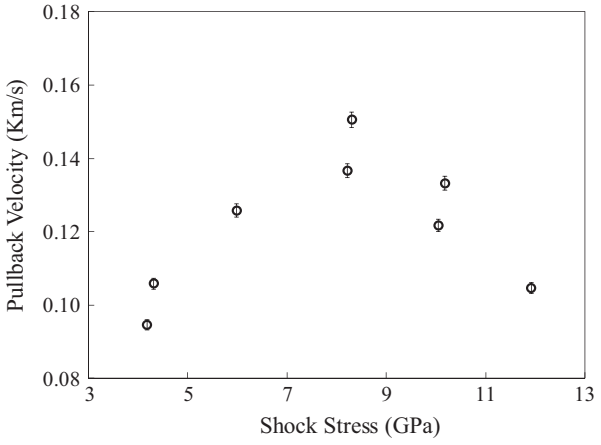

Fig. 1. Comparison between the spall response of 1100-O and 1060 aluminum [18–19]. Error bars denotes precision associated with VISAR free surface velocity measurements.

The density and elastic wave speeds of the 1100-O aluminum were also previously measured by Williams et al. [20,21], and these values were used to compute the elastic properties. The density measurements were made using Archimedes principle and the elastic wave speeds were measured using non-destructive ultrasonic techniques [20,21]. The resulting measurements and their associated standard deviation as obtained by Williams et al. [20,21] are listed in Table 2.

3. Experimental methods

Studies of the effects of shock waves on the structure and properties of materials can be traced back to the work of Smith [22] in the late 1950s using recovery plate impact experiments. This approach has since proven to be extremely useful in studying the effects of parameters such as peak shock stress [7–15,23], pulse duration [7,10,24–27], grain size [11,28,29], stacking fault energy [11], and temperature [11] on the substructural evolution in metals. Therefore, recovery plate impact experiments are employed in this research to study the effects of shock stress on the substructure evolution and subsequent spall fracture of 1100-O aluminum. Detail descriptions of the shock recovery plate impact technique can be found in DeCarli and Meyers [30] and Gray [31].

All plate impact recovery experiments for this investigation were conducted using a single stage 102 mm diameter (slotted bore) gas gun at the shock physics laboratory, U.S. Army Research Laboratory (ARL), Aberdeen Proving Ground (APG). A series of four charged pins were used to determine the flyer velocity prior to impacting the target. The uncertainty associated with the pin positions was determined to be less than 1.0×10^{-4} m, corresponding to an uncertainty associated with the final velocity of the flyer of less than 2%. Plate impact was determined (using laser alignment) to be normal to within 0.5 mrad of tilt.

A 2 mm thick and 43 mm diameter tungsten carbide (WC) flyer mounted on a sabot is accelerated into a stationary aluminum target (sample) assembly using the light gas gun resulting in a non-symmetric impact. The basic loading configuration is shown in Fig. 3 [32,33]. In general, symmetric impacts are preferable to non-symmetric impacts because the resulting wave interactions are simpler to analyze. However, WC flyers were used for this experimental study so that the required shock stresses (ranging from 4 to 9 GPa) could be attained at relatively low impact velocities compared to those for symmetric impacts. Low impact velocities minimize the complexities associated with the soft recovery process (in particular secondary impacts). The thickness

Table 1
Elemental composition and percent weight for Al 1100-O alloy.

Element	*% Weight*	*Element*	*% Weight*	*Element*	*% Weight*
Al	99.0	Cu	0.15	Cr	0.01
Si	0.15	Mn	0.01	Zn	0.01
Fe	0.51	Mg	0.01	Ti	0.015

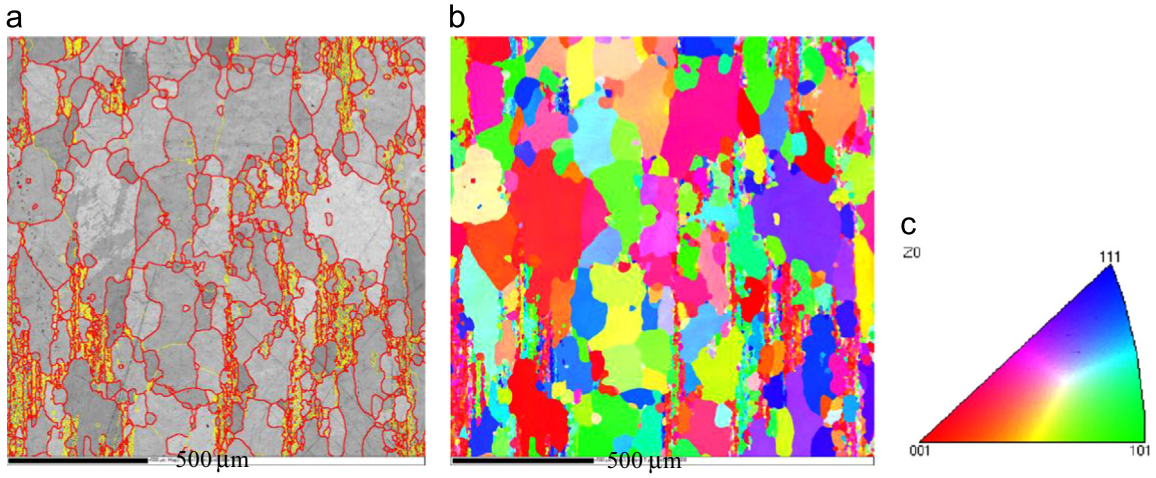

Fig. 2. EBSD results for 1100-O aluminum (a) grain boundary map, (b) grain orientation map, and inverse pole figure (c). (For interpretation of the references to color in this figure, the reader is referred to the web version of this article.)

Table 2
Density and elastic properties of 1100-O aluminum alloy.

Parameters	*Al 1100-O Alloy*
Density (ρ_0)	2710.10 ± 1.40 *Kg/m³*
Longitudinal Wave Velocity (C_L)	6451.68 ± 12.47 *m/s*
Shear Wave Velocity (C_S)	3132.30 ± 10.57 *m/s*
Bulk Wave Velocity (C_B)	5342.53 ± 15.77 *m/s*
Shear Modulus (μ)	26.59 ± 0.19 *GPa*
Elastic Modulus (E)	71.57 ± 0.44 *GPa*
Bulk Modulus (K)	77.35 ± 0.47 *GPa*
Lame's Modulus (λ)	59.63 ± 0.52 *GPa*
Poisson's Ratio (ν)	0.33

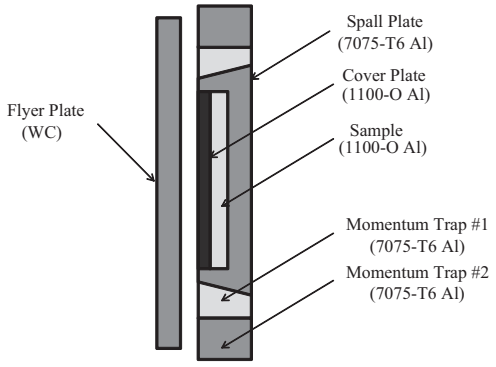

Fig. 3. Plate-impact loading configuration used for both shock and spall recovery experiments.

of the WC flyer was selected to match the approximate pulse duration employed by Williams et al. [19,20] using symmetric impacts. The pulse duration for the 2 mm thick WC flyer was approximately 0.8 µs and that employed by Williams et al. [19,20] was approximately 1.0 µs. The pulse durations were estimated using $t_p = \frac{2d^D}{U_s^D}$, where d^D is the flyer plate thickness and U_s^D is the shock velocity in the flyer plate. The properties of the WC flyers were previously reported by Dandekar and Grady [34]; the Hugoniot elastic limit (*HEL*), density (ρ_0), longitudinal wave speed (C_L), shear wave speed (C_S), and bulk sound speed (C_0), were determined to be 6.6 GPa, 15,530 kg/m^3, 7.050 km/s, 4.320 km/s, and 4.980 km/s respectively.

Two distinct types of plate impact recovery experiments (shock-release and shock-release-spall) were conducted in order to interrogate the substructure evolution and spall fracture surfaces of the 1100-O aluminum. Shock-release recovery experiments will be referred to as shock recovery experiments from this point forward, while shock-release-spall experiments will be referred to as spall recovery experiments. For shock recovery experiments, the sample undergoes shock compression and release. On the other hand, for spall recovery experiments the sample undergoes shock compression, release, and then spall. Five plate impact recovery experiments were conducted on 1100-O aluminum (3-shock and 2-spall). Shock recovery experiments were conducted at shock stresses of approximately 4, 6, and 9 GPa to study the substructure evolution, while spall recovery experiments were conducted at shock stresses of approximately 6 and 9 GPa to study the spall fracture surfaces. As shown in Fig. 3, a 4 mm thick by 30 mm diameter recovery sample is seated in a cavity within a sacrificial spall plate, which is fabricated from 7075-T6 aluminum. The 7075-T6 aluminum was chosen primarily because of its increased toughness which protects the 1100-O aluminum during the soft recovery process. The 1100-O sample is tightly sandwiched inside the spall plate cavity by a cover plate fabricated from 1100-O aluminum for increased protection during the soft recovery process. Two concentric momentum trapping rings (also fabricated from 7075-T6 Al) with outer diameters of 40 mm and 45 mm were used for trapping radial release waves. The sacrificial

spall plate has a 7° taper angle so that it can be easily separated from the momentum trapping rings after impact. For spall recovery experiments, the sacrificial spall plate was fabricated from 1100-O aluminum. This configuration allows for the rarefaction waves from opposite free surfaces (WC flyer and 1100-O aluminum spall plate) to interact and induce spall failure.

After impact, the target assembly is launched into a catch tank while the sabot and trapping rings are stripped by a high strength steel specimen holder in the test chamber (see Fig. 4). The target assembly first travels through a series of structural foams stacked in sequence from low to high density in the test chamber to decelerate the target assembly in a gradual manner. This minimizes the detrimental effects of secondary impacts which may possibly change the microstructure achieved at the shock state. As soon as the target assembly enters the catch tank, it goes through a cylindrical block (406 mm diameter by 914 mm long) of chilled ballistic foam mounted inside a tubing (aluminum). The ballistic foam further decelerates the target assembly and prevents detrimental secondary impacts during soft recovery. The ballistic foam is chilled to an average temperature of 9 °C and is also used for quenching the test assembly and hence, prevents static recovery while the specimen is in the catch tank awaiting retrieval. The recovered sample is then retrieved for sectioning and microstructural examination. This target design and recovery approach has been previously employed in earlier shock recovery plate impact experiments involving aluminum and other metallic materials [2], [32,33].

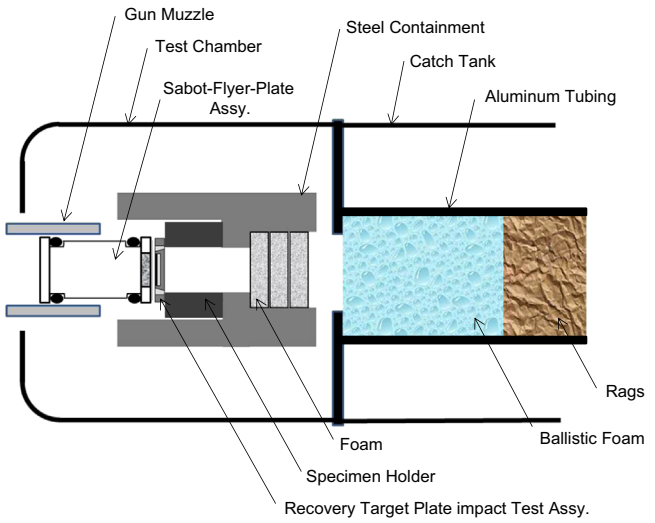

Fig. 4. An illustration of the plate impact recovery test setup used for both shock and spall recovery experiments.

The microstructures of the recovered 1100-O aluminum samples were characterized using field-emission-gun transmission electron microscopy (FEG-TEM; Philips EM 300) and scanning electron microscopy (EI 600i Nova NanoLab dual beam). All TEM samples were sectioned using wire electro-discharge machining (EDM) along the through-thickness direction. The samples were first mechanically polished and then electropolished using a solution consisting of 25 vol% HNO_3 and 75% methanol at different voltages ranging from 6–60 V in a TenuPol-3 digitally controlled automatic electropolisher. The hardness of the recovered samples was measured using a Wilson Tukon model 300 with a Vickers diamond indenter and was calibrated with a Wilson standard test block.

4. Results and discussion

The spall response of 1100-O aluminum obtained by Williams et al. [20,21] is shown in Fig. 1. Williams et al. [20,21] determined that as the peak shock stress is increased up to approximately 8.3 GPa, the pullback velocity increases likely due to shock hardening of the material. However, when the peak shock stress is further increased beyond 8.3 GPa, the pullback velocity decreases possibly due to work softening induced by dynamic recovery which is a direct consequence of thermally-activated microstructural reorganization. Williams et al. [20,21] suspected a likely competition between dislocation generation (shock hardening) and temperature assisted microstructural reorganization (dynamic recovery) to be at play in Fig. 1.

The substructure of the as-received 1100-O aluminum was first characterized using a transmission electron microscope (TEM) as shown in Fig. 5. Although the average grain size was previously determined to be approximately 250 μm (see Fig. 2), however, the micrograph shown in Fig. 5(a) represents an area with clusters of small grains which are more or less equiaxed. On average, the interior of the large grains were free of low angle boundaries (Fig. 2(a)). An enlarged view of the grain labeled A in Fig. 5(a) is shown in Fig. 5(b) and discrete dislocations are evident in the interior of the grain. The presence of discrete dislocations within the grains is consistent with the fact that annealed materials are expected to have dislocation densities on the order of 10^{12} m^{-2} [35]. This also suggests a history of prior mechanical processing such as rolling, extrusion, or forging.

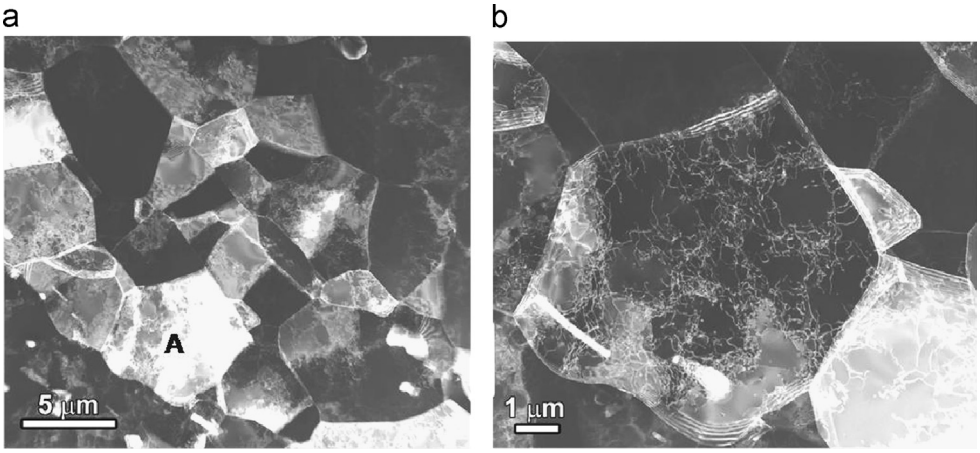

Fig. 5. TEM micrographs of the as-received 1100-O aluminum (a) and a magnified view of the grain labeled A (b).

4.1. Shock and release recovery experiments

We now examine the microstructure of the shock-recovered samples. Note that all TEM micrographs were obtained from the mid-section of the sample which represents the through-thickness of the shocked material. Micrographs of the substructure of 1100-O aluminum shocked at 4 GPa are shown in Fig. 6. Fig. 6(a) shows that the original equiaxed grains have evolved into severely elongated sub-grains with cells in their interior when shock loaded to 4 GPa. Also evident in Fig. 6(a) are misorientations between neighboring sub-grains because of the distinct contrast between sub-grains. Slightly tangled dislocation substructures also begin to develop in the interior of the sub-grains as shown in Fig. 6 (b). Dislocation debris (denoted DD) is also observed to be uniformly distributed throughout the micrograph (Fig. 6(b)). We note here that Gray and Follansbee [8] have previously observed dislocation debris in 6061-T6 aluminum shocked at 2 GPa. Dislocation debris is a direct consequence of the double cross-slip mechanism [36,37].

The substructure of 1100-O aluminum shock loaded to 6 GPa (Fig. 7) is distinctly different from that shocked at 4 GPa as shown in Fig. 6. The starting microstructure has evolved into densely packed cell blocks delineated by dense dislocation walls (DDWs: denoted by D) and microbands (MBs: denoted by M) as shown in Fig. 7(a). Cell block boundaries (DDWs and MBs) accommodate the strain mismatch between cell blocks and are therefore referred to as geometrically necessary boundaries (GNBs) [38]. The formation of DDWs and MBs in plastically deformed aluminum has been described previously by Hansen [38] and Bay et al. [39]. A magnified view of the interior of a cell block is shown in Fig. 7(b) and it reveals a substructure of discrete dislocations and dislocation debris similar to that obtained at 4 GPa.

For a shock stress of 9 GPa, the starting microstructure evolves into a plate-like lamellar structure as shown in Fig. 8(a). The lamellar structure exhibits long strips with flat boundaries (denoted by L) running almost parallel to each other with a single cell block spanning across them. Observed in Fig. 8(b) are aggregated dislocations and dislocation debris similar to those observed at 4 and 6 GPa peak shock stress. These results show a substantial evolution of the microstructure with increase in peak shock stress.

4.1.1. Post shock hardness measurements

Three microhardness measurements were taken respectively from both the impact (shocked) and through-thickness planes of the shock recovered samples in order to determine the residual hardness. The results (Fig. 9) show that the residual hardness measured from both the impact and mid-point of the through-thickness plane increases almost linearly as a function of the peak shock stress with the largest increase occurring between 6 GPa and

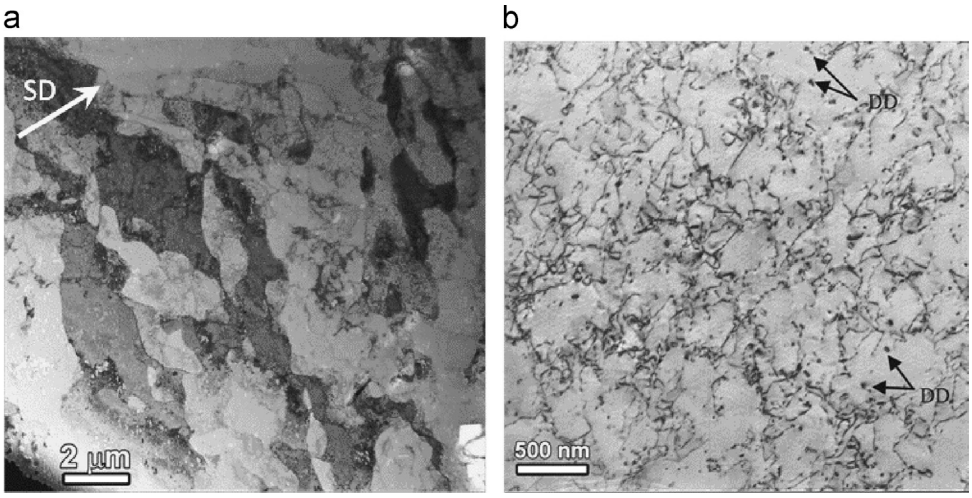

Fig. 6. TEM micrographs of the 1100-O aluminum shocked at 4 GPa with arrow (SD) indicating shock direction (a) and a magnified view of the substructure (b).

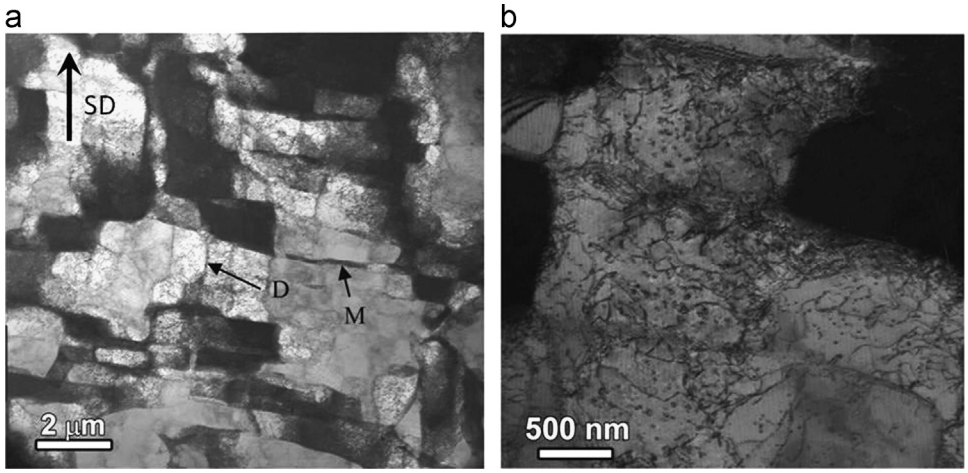

Fig. 7. TEM micrographs of the 1100-O aluminum shocked at 6 GPa with arrow (SD) indicating shock direction (a) and a magnified view of the substructure (b).

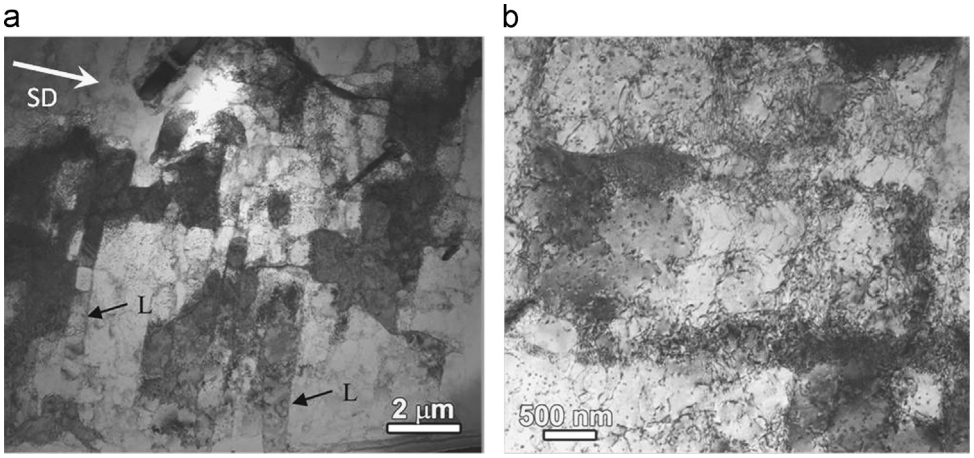

Fig. 8. TEM micrographs of the 1100-O aluminum shocked at 9 GPa (a) and a magnified view of the substructure with arrow (SD) indicating shock direction (b).

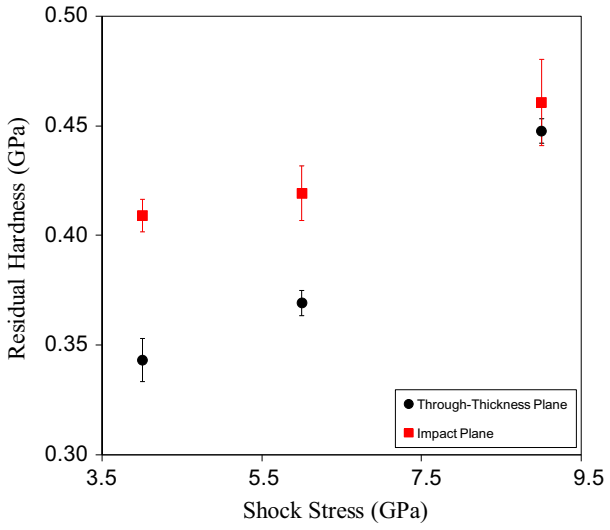

Fig. 9. Residual hardness as a function of peak shock stress of 1100-O aluminum (through thickness and impact planes). Error bars denotes standard deviation.

9 GPa. Measurements taken from the impact surface were consistently higher than those taken at the mid-point of the through-thickness plane. However, the difference in hardness between both planes decreases with increase in shock stress.

At a shock stress of 9 GPa, the hardness measurements taken from both planes closely approach each other. This difference in hardness between the impact and through-thickness planes is possibly due to shock wave attenuation [40]. The rarefaction rate decreases through the thickness of the material or as the shock wave travels through the thickness of the specimen, it attenuates itself and therefore, exhibits a lower hardness in the interior of the sample as compared to the impact surface.

The hardness results are consistent with the empirical relationship in Eq. (1) [11], which implies that the post-shock yield strength increases with increase in dislocation density, decrease in cell size, and decrease in twin spacing.

$$\sigma = \sigma_0 + \alpha\mu b\sqrt{\rho} + K_1 d^{-1} + K_2 \Delta^{-1/2} \quad (1)$$

where σ_0 is the preshock yield strength, ρ is the dislocation density, $K_1$and K_2 are material parameters, α is a constant ($\sim$0.5), μ is the shear modulus, Δ is the twin spacing, and b is the magnitude of the Burgers vector. The twin spacing term in Eq. 1 is usually neglected for polycrystalline pure aluminum, because the critical twinning shock stress of aluminum is very high ($\sim$40 GPa according to Murr [41]). This is well above the shock stress range employed in this study and is also supported by the fact that deformation twins are not generally observed in polycrystalline aluminum shock loaded at room temperature. At approximately 40 GPa, the residual temperature is estimated to be approximately 300 °C [41] (the melting temperature of aluminum is 660 °C) and this suppresses the formation of twins. However, the dislocation density usually increases with shock stress, and the cell size usually decreases with shock stress, therefore, Eq. (1) suggests that increasing the peak shock stress will result in an increase in the post-shock yield strength and hence residual hardness of the 1100-O aluminum. Previous observations from experiments support the fact that increasing the peak shock stress does lead to increases in the post shock yield strength and residual hardness of metals [11,12,31,41,42].

The observed increase in hardness as a function of shock stress eliminates thermal softening as operative between 4 GPa and 9 GPa. The Hugoniot temperatures were calculated as a function of shock stress for aluminum (Fig. 10) using the Mie–Gruneisen Equation of State (EOS) [5]. The results show that the Hugoniot temperatures achieved at 4, 6, and 9 GPa were approximately 331 K, 349 K, and 379 K respectively. The highest Hugoniot temperature achieved (at $\sim$9 GPa shock stress) corresponds to about $0.4T_m$ (T_m is the absolute melting temperature). Although this increase in Hugoniot temperature may not be high enough to induce thermal softening, however, it does contribute strongly to the substructure reorganization as previously described. This reorganization may change the active deformation mechanism between 6 GPa and 9 GPa. This change according to Williams et al. [20,21] was likely induced by dynamic recovery.

4.1.2. Shock induced dynamic recovery

Dynamic recovery involves the annihilation of dislocations by glide and cross-slip in mixed sub-boundaries. It is strongly influenced by thermal activation but can also occur mechanically, in principle even at absolute zero temperature [43]. However, at low temperatures climb is not significant and therefore, edge dislocations cannot annihilate [43]. With increase in stress and temperature, edge dislocations not only begin to diffuse but combine to form edge dipoles. Previously stored dislocations are reorganized under the action of stress, temperature, and strain rate into lower energy configurations such as dipoles and incipient sub-boundaries [43]. This reorganization is primarily responsible for dynamic recovery. Furthermore, changing either the stress, temperature, or strain rate can influence the degree of reorganization in the deformed material [44]. These reorganizations are usually reflected in the substructure of the dynamically recovered

material. For instance, increases in the residual dislocation debris within the cell interior and/or suppression of dislocation cells are both manifestations of the thermally activated nature of dynamic recovery [44–47]. The activation energy required for cross slip is inversely proportional to the stacking fault energy and decreases logarithmically with stress according to Eq. (2) [47–49].

$$\Delta G = -\frac{E_Q^2}{\gamma}\ln\left(\frac{\tau}{\tau_Q}\right) \tag{2}$$

where γ is the stacking fault energy, τ is shear stress, E_Q and τ_Q are constants. In addition, the activation energy required for cross slip is expected to increase with increase in temperature but decreases with increase in strain rate as stated in Eq. (3) [50]. Therefore, metals with high stacking fault energy such as aluminum ($\sim$200 mJ/m^2) require low activation energy for cross-slip [5] and are therefore predisposed to favor dynamic recovery [48]. Dynamic recovery usually manifests itself as work softening [51].

$$\Delta G = AkT\ln\left(\frac{\nu_{cs}}{\dot{\gamma}}\right) - \frac{kT}{\mu b^3}\tau V \tag{3}$$

where A is constant and is approximately 1, k is the Boltzmann constant, T is temperature, ν_{cs} is the frequency for cross-slip, μ is the shear modulus, b is the magnitude of the Burger's vector, τ is the applied shear stress, and V is the activation volume.

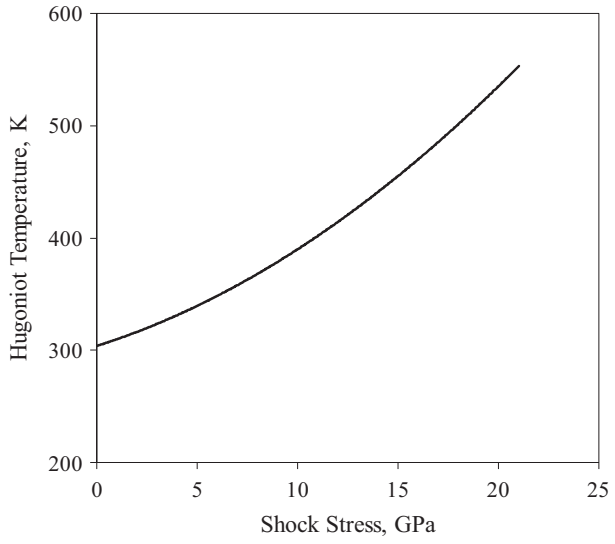

Fig. 10. Hugoniot temperature calculated as a function of peak shock stress for aluminum using the Mie–Gruneisen equation of state [5].

The preponderance of the evidence obtained from the substructure evolution of 1100-O aluminum in conjunction with microhardness results suggest that perhaps shock hardening was likely the dominant mechanism up to approximately 8.3 GPa and softening induced by dynamic recovery likely became dominant beyond 8.3 GPa. The starting microstructure consisting of equiaxed grain with tangles within the interior evolved to elongated grains with a uniformly distributed dislocation structure and dislocation debris after being shocked to 4 GPa shock stress. The likely increase in dislocation density is primarily responsible for the hardening and is supported by hardness measurements on the shocked samples (Fig. 9). In addition, the dislocation debris left in the wake of the advancing dislocations also acts as a hardening agent [36]. That is, the debris become obstacles to the trailing dislocations and are believed to cause self hardening [36,37]. Although the mechanism of dislocation debris hardening is not fully understood, their contribution to the total hardening is suggested to be probably small [37].

4.2. Spall recovery experiments

The fracture surfaces from spall recovery experiments were analyzed using a scanning electron microscope (SEM). The micrograph in Fig. 11(a) shows the fracture surface of the sample after spall failure following a 6 GPa shock stress. The figure shows that the fracture surface is of the classic ductile type dominated by dimples [52]. The dimples are fairly rounded, suggesting that the stress was approximately hydrostatic [52]. The diameter of the microvoid dimples ranges from approximately 8 μm to 25 μm. Microvoids penetrate deep (approximately 550 μm) into the material as shown in Fig. 11(b). The figure also reveals a rough edge throughout the entire length of the fracture surface. This is consistent with surfaces produced by ductile transgranular spall fracture and has been previously observed in laser shocked aluminum [53].

Fig. 12(a) which was obtained at the same magnification as compared to Fig. 11(a) shows the fracture surface resulting from the 9 GPa shock stress. Remarkably, the fracture surface is of the brittle type and no microvoids are visible. This type of surface is indicative of a brittle intergranular fracture [52] by decohesion. A magnified view of the fracture surface is shown in Fig. 12(b) and reveals a fairly smooth region with flaps of material normally referred to as tongues that are characteristic of brittle fracture [52]. Such features were previously observed by Dalton et al. [54] in laser shocked aluminum. No microvoids were observed on the fracture surface. However, at a magnification of 80,000 ×, nanovoids were observed at isolated regions on the fractured surface (see Fig. 12(c)). The diameter of the nanovoid dimples ranges from approximately 38 nm to 125 nm. This observation suggests a

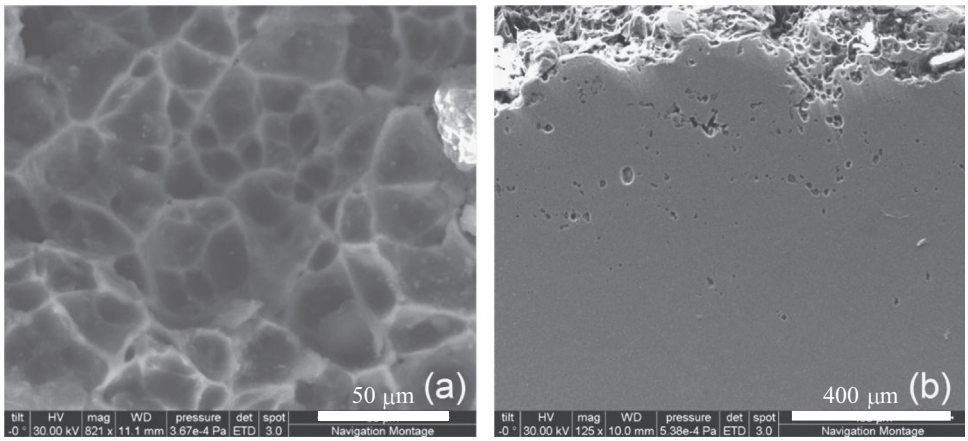

Fig. 11. SEM micrographs of the 1100-O aluminum shocked at 6 GPa showing (a) dimples on the fracture surface, (b) the cross-sectional view of the fractured sample.

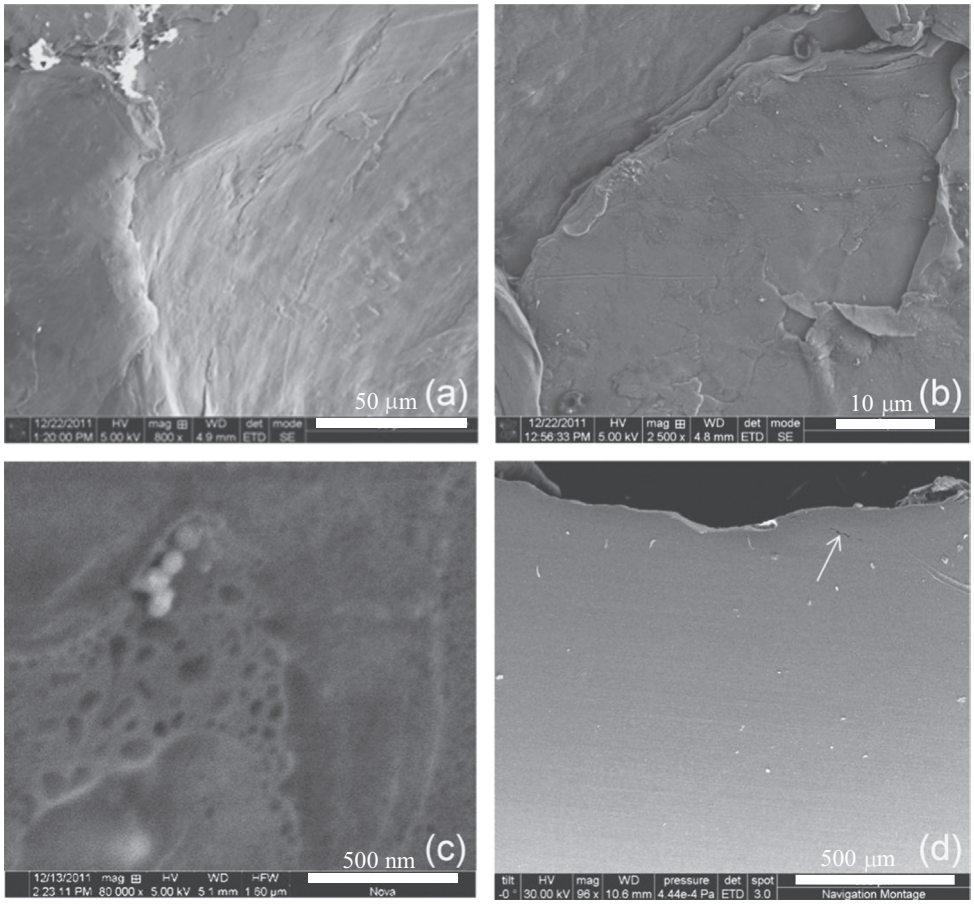

Fig. 12. SEM micrographs of the 1100-O aluminum shocked at 9 GPa showing (a) intergranular spall fracture surface, (b) an enlarged view of the intergranular spall fracture surface with tongues, (c) nanovoids in isolated areas of the fracture surface, and (d) the cross-sectional view of the fractured sample.

quasi-brittle failure consisting of both brittle intergranular failure and ductile transgranular failure with brittle intergranular failure being the dominant mode. Quasi-brittle failure surfaces were previously observed in laser shocked aluminum by Brewer et al. [53] and Dalton et al. [54].

Furthermore, no voids were observed on the sectioned surface of the material shocked at 9 GPa; however, a macrocrack below the fractured surface was evident as shown by the arrow in Fig. 12 (d). The fracture surface throughout the entire length of the cross-section is relatively flat when compared to that acquired at 6 GPa. This type of fractured surface is consistent with those produced by brittle intergranular spall fracture [53,54].

The ductile transgranular spall failure observed at 6 GPa is due to void nucleation, growth, and coalescence. Spall failure occurs within the tensile zone and the zone size was estimated to be at a minimum about 1100 μm (1.1 mm) wide. This estimate was derived from the fact that voids were observed approximately 550 μm below the fracture surface as shown in Fig. 11(b) and with symmetry taken into consideration; a similar observation should be expected above the spall plane. With this estimate, it is clear from Fig. 7(a) that the tensile zone spans multiple cell blocks. The vast majority of dislocation interactions occur at cell block boundaries and therefore, these boundaries are potential void nucleation sites. Spall failure occurs at very high unloading rates ($\sim 10^5\ s^{-1}$) [20,21] and preferentially follow the path that requires the least energy to induce failure. In commercially pure metals such as in this case, voids nucleated at precipitates are difficult to grow and coalesce because of their relatively large separation distance. In addition, fewer precipitates congregate at grain boundaries and therefore, increase the resistance to void nucleation, growth, and coalescence and hence spall resistance [55]. But in some cases where the orientation of the subgrain boundary is almost parallel to the tensile loading direction, less energy may be required to induce failure within the sub-grain than that required for boundary failure. Consequently, the spall failure will occur along sub-grain boundaries and their interior producing jagged edges (Fig. 11(b)).

On the other hand, sub-grains with boundaries aligned parallel to the spall plane or perpendicular to the tensile loading direction will likely induce fracture along the boundary. Failure has been known to preferentially follow grain and sub-grain boundaries [54] which makes grain size and shape [53,54] important factors in spall fracture. Grain boundaries are planar defects and perhaps the path of least resistance; therefore, less energy may be required to induce spall at boundaries that are aligned normal to the tensile loading direction as oppose to nucleating, growing, and coalescing voids in the interior of the grain. This is consistent with the pullback velocity (spall strength) acquired at 9 GPa (less than that acquired at 6 GPa.)

At 9 GPa shock stress, the starting microstructure has evolved into lamellar structures whose grain boundaries are almost parallel to the spall plane and almost orthogonal to the tensile loading direction. This grain evolution induces intergranular fracture by decohesion along the weak grain boundary which is a low energy fracture mode [48]. Intergranular decohesion is likely responsible for the flat smooth fracture surface observed in Fig. 12. Furthermore, although the residual hardness at 9 GPa is higher than that at 6 GPa suggesting an increase in hardening, substructure reorganization (dynamic recovery) may be the dominant mechanism.

In addition to intergranular decohesion, another plausible explanation for the reduction in pullback velocity (spall strength) beyond 8.3 GPa peak shock stress is texture softening. Under shock loading

conditions, if the grains within the lamellar boundaries are rotated towards crystallographic orientations for which the Schmid factor is increased, then the material will geometrically soften regardless of the increase in residual hardness. This plausible explanation needs to be confirmed by an in depth texture analysis of the shocked 1100-O aluminum samples. The contributions of nanovoids to the dynamic recovery process are not fully understood and clearly deserve further investigations.

5. Conclusions

This research shows that the substructure of the 1100-O aluminum evolves substantially with increase in peak shock stress ranging from 4 GPa to 9 GPa. Substructural evolution in conjunction with microhardness and spall failure results suggest that shock hardening was perhaps due to increase in dislocation density and ductile fracture by void nucleation, growth, and coalescence was possibly the dominant failure mode up to 8.3 GPa. Beyond 8.3 GPa, softening was perhaps induced by dynamic recovery and brittle intergranular fracture by decohesion with isolated pockets of nanovoids was possibly the dominant fracture mode. The contributions of nanovoids to the dynamic recovery process, if any, require further investigations. Microhardness measurements show an increase in residual hardness throughout the shock stress range studied, suggesting shock hardening. This observation also suggests that thermal softening was not operative throughout the shock stress range studied. However, dynamic recovery was thermally influenced during shock loading. Texture analyses on the shocked samples are needed to study the role of texture softening, if any.

Acknowledgments

Funding for this research was provided by both the United States Army Research Laboratory (ARL) at Aberdeen Proving Ground and the Center for Advanced Metallic and Ceramic Systems (CAMCS) at The Johns Hopkins University under ARMAC-RTP Cooperative Agreement no. W911NF-06-2-0006. The authors wish to acknowledge Dr. George "Rusty" Gray III (Los Alamos National Laboratory) for his valuable technical suggestions with regards to the recovery experiments and Dr. John D. Clayton for reviewing the manuscript.

References

[1] T. Antoun, L. Seaman, D.R. Curran, G.I. Kanel, S.V. Razorenov, A.V. Utkin, Spall Fracture, Springer-Verlag, New York, 2003.
[2] G.T. Gray III, Influence on shock-wave deformation on the structure/property behavior of materials, in: J.R. Asay, M. Shahinpoor (Eds.), High-Pressure Shock Compression of Solids, Springer-Verlag, New York, 1993, p. 187.
[3] G.T. Gray III, J.C. Huang, Mater. Sci. Eng. A145 (1991) 21.
[4] G.T. Gray III, Acta Metall. A145 (1988) 1745.
[5] M.A. Meyers, Dynamic Behavior of Materials, John Wiley and Sons, New York, NY, 1994.
[6] H. Kressel, N. Brown, J. Appl. Phys. 38 (1967) 1618.
[7] L.E. Murr, The effects of peak pressure, pulse duration, and repeated loading on the residual structure and properties of shock deformed metals and alloys, in: M.A. Meyers, L.E. Murr (Eds.), Shock Waves and High-Strain-Rate Phenomena in Metals, Plenum, New York, 1981, p. 753.
[8] G.T. Gray III, P.S. Follansbee, Influence of peak pressure on substructure evolution and mechanical response of shock-loaded 6061-T6 aluminum, in: S.C. Schmidt, N.C. Holmes (Eds.), Shock Waves in Condensed Matter 1987, Elsevier Science, New York, 1988, p. 339.
[9] G.T. Gray III, C.E. Morris, Influence of peak pressure on the substructure evolution and shock wave profiles of Ti–6Al–4V, in: P. Lacombe, R. Tricot, G. Beranger (Eds.), Sixth World Conference on Titanium, Les Editions de Physique, France, 1989, p. 269.
[10] G.T. Gray III, P.S. Follansbee, Influence of peak pressure, pulse duration, and repeated loading on substructure development and threshold stress in shock-loaded copper, in: C.Y. Chiem, H.D. Kunze, L.W. Meyer (Eds.), Impact Loading and Dynamic Behavior of Materials, Deutsche Gesellschaft fuer Metalkunde, Germany, 1988, p. 541.
[11] L.E. Murr, Residual microstructure–mechanical property relationships in shock-loaded metals and alloys, in: M.A. Meyers, L.E. Murr (Eds.), Shock Waves and High Strain Rate Phenomena in Metals, Plenum, New York, 1981, p. 607.
[12] L.E. Murr, Metallurgical effects of shock and high strain rate loading, in: T.Z. Blazynski (Ed.), Materials at High Strain Rates, Elsevier/Applied Science, London, 1987, p. 1.
[13] W.C. Leslie, Microstructural effects of high strain rate deformation, in: R.W. Rohde, B.M. Butcher, J.R. Holland, C.H. Karners (Eds.), Metallurgical Effects at High Strain Rates, Plenum, New York, 1973, p. 571.
[14] G.E. Dieter, Metallurgical effects of high-intensity shock waves in metals, in: P.G. Shewmon, V.F. Zackey (Eds.), Response of Metals to High Velocity Deformation, Interscience, New York, 1961, p. 409.
[15] K.P. Staudhammer, Shock wave effects and metallurgical parameters, in: C.Y. Chiem, H.D. Kunze, L.W. Meyer (Eds.), IMPACT 1987, Duetsche Gesellschaft fur Metallkunde, Oberursel, West Germany, 1988, p. 93.
[16] M.A. Meyers, L.E. Murr, Defect generation in shock-wave deformation, in: M.A. Meyers, L.E. Murr (Eds.), Shock Waves and High-Strain-Rate Phenomena in Metals, Plenum, New York, 1981, p. 487.
[17] J.C.F. Millett, M. Cotton, N.K. Bourne, N.T. Park, G. Whiteman, J. Appl. Phys. 115 (2014) 073506.
[18] D.E. Gray, J.R. Asay, J. Appl. Phys. 53 (1982) 7350.
[19] X. Chen, J.R. Asay, S.K. Dwivedi, D.P. Field, J. Appl. Phys. 99 (2006) 023528.
[20] C.L. Williams, K.T. Ramesh, D.P. Dandekar, J. Appl. Phys. 111 (2012) 123528.
[21] C.L. Williams, C.Q. Chen, K.T. Ramesh, D.P. Dandekar, J. Appl. Phys. 114 (2013) 093502.
[22] C.S. Smith, AIME 212 (1958) 574.
[23] A.S. Appleton, Appl. Mater. Res. 7 (1965) 195.
[24] A.S. Appleton, J.S. Waddington, Acta Metall. 12 (1964) 956.
[25] R.N. Wright, D.E. Mikkola, Metall. Trans. 16A (1985) 881.
[26] D.E. Mikkola, R.N. Wright, Dislocation generation and its relation to the dynamic plastic response of shock loaded metals, in: J.R. Asay, R.A. Graham, G.K. Straub (Eds.), Shock Waves in Condensed Matter – 1983, Elsevier Science, New York, 1984, p. 415.
[27] B. Kazmi, L.E. Murr, Scr. Metall. 13 (1979) 993.
[28] M.A. Meyers, U.R. Andrade, A.H. Chokshi, Metall. Mater. Trans. A 26A (1995) 2881.
[29] H.J. Kestenbach, M.A. Meyers, Metall. Mater. Trans. A 7A (1976) 1943.
[30] P.S. DeCarli, M.A. Meyers, Design of uniaxial strain shock recovery experiments, in: M.A. Meyers, L.E. Murr (Eds.), Shock Waves and High-Strain-Rate Phenomena in Metals, Plenum, New York, 1981, p. 341.
[31] G.T. Gray III, Shock recovery experiments: an assesment, in: S.C. Schmidt, J.N. Johnson, L.W. Davison (Eds.), Shock Compression of Condensed Matter – 1989, Elsevier Science, Amsterdam, 1990, p. 407.
[32] N.K. Bourne, G.T. Gray III, Proc. R. Soc. A 461 (2005) 3297.
[33] N.K. Bourne, G.T. Gray III, J.C.F. Millett, J. Appl. Phys. 106 (2009) 091301.
[34] D.P. Dandekar, D. Grady, Shock equation of state and dynamic strength of tungsten carbide, in: M.D. Furnish, N.N. Thadani, Y. Horie (Eds.), Shock Compression of Condensed Matter – 2001, American Institute of Physics, New York, 2002, p. 783.
[35] M.A. Meyers, K.K. Chawla, Mechanical Behavior of Materials, Cambridge University Press, New York, 2009.
[36] J.J. Gilman, J. Appl. Phys. 33 (1962) 2703.
[37] U. Messerschmidt, Dislocation Dynamics During Plastic Deformation, Springer-Verlag, Berlin, 2010.
[38] N. Hansen, Mater. Sci. Technol. 6 (1990) 1039.
[39] B. Bay, N. Hansen, D. Kuhlmann-Wilsdorf, Mater. Sci. Eng. A158 (1992) 139.
[40] M.A. Meyers, L.E. Murr, C.Y. Hsu, G.A. Stone, Mater. Sci. Eng. 57 (1983) 1139.
[41] L.E. Murr, Shock Waves for Industrial Applications, Noyes Publications, New Jersey, 1988.
[42] G.T. Gray III, Shock experiments in metals and ceramics, in: M.A. Meyers, L.E. Murr, K.P. Staudhammer (Eds.), EXPLOMET 90, Marcel Dekker, New York, 1991.
[43] U.F. Kocks, Dislocation interactions: flow stress and strain hardening, in: Proceedings of the Conference on Dislocations and Properties of Real Materials, London, 1985.
[44] U. Essmann, H. Muhgrabi, Philos. Mag. 40 (1979) 731.
[45] G.T. Gray III, Deformation Substructures Induced by High-Rate Deformation, Los Alamos Report LA-UR-91-610, 1991.
[46] J. Gil Sevillano, P. van Houtte, E. Aernoudt, Prog. Mater. Sci. 25 (1981) 174.
[47] F. Cheval, L. Priester, Scr. Metall. 23 (1989) 1871.
[48] R.J. Amodeo, N.M. Ghoniem, Res. Mech. 23 (1988) 137.
[49] P. Haasen, Physical Metallurgy, Cambridge University Press, New York, 1996.
[50] M. Huang, P.E.J. Rivera-Diaz-del-Castillo, O. Bouaziz, S. van der Zwagg, Mech. Mater. 41 (2009) 982.
[51] T.H. Alden, Metall. Trans. A 7A (1976) 1057.
[52] C.R. Brooks, A. Chowdhury, Metallurgical Failure Analysis, McGraw-Hill, New York, 1993.
[53] J.L. Brewer, D.A. Dalton, E.D. Jackson, A.C. Bernstein, W. Grigsby, E.M. Taleff, T. Ditmire, Metall. Mater. Trans. A 38A (2007) 2666.
[54] D.A. Dalton, J.L. Brewer, A.C. Bernstein, W. Grigsby, D. Milathianaki, E.D. Jackson, R.G. Adams, P. Rambo, J. Schwartz, A. Eldens, M. Geissel, I. Smith, E.M. Taleff, T. Ditmire, J. Appl. Phys. 104 (2008) 013526.
[55] Y. Wang, M. Qi, H. He, L. Wang, Mech. Mater. 69 (2014) 270.

1 (PDF) DEFENSE TECHNICAL INFORMATION CTR DTIC OCA

2 (PDF) DIRECTOR US ARMY RESEARCH LAB RDRL CIO LL IMAL HRA MAIL & RECORDS MGMT

1 (PDF) GOVT PRINTG OFC A MALHOTRA

2 (PDF) THE JOHNS HOPKINS UNIV CQ CHEN KT RAMESH

39 (PDF) DIR USARL
RDRL CIH C
P CHUNG J KNAP
RDRL WM
B FORCH
J MCCAULEY
RDRL WML B
I BATYREV
B RICE
D TAYLOR
N WEINGARTEN
RDRL WML H
B SCHUSTER
RDRL WMM
J BEATTY
RDRL WMM B
G GAZONAS
D HOPKINS
B POWERS
RDRL WMM E
J SWAB
RDRL WMM F
C DARLING
L KECSKES
T SANO
M TSCHOPP
RDRL WMM G
J ANDZELM
RDRL WMP
S SCHOENFELD
RDRL WMP A
S BILYK
RDRL WMP B
C HOPPEL
A SOKOLOW
S SATAPATHY
M SCHEIDLER
T WEERISOORIYA
RDRL WMP C
R BECKER
T BJERKE
D CASEM
J CLAYTON
D DANDEKAR
M GREENFIELD
R LEAVY
J LLOYD
S SEGLETES
A TONGE
C WILLIAMS
RDRL WMP D
R DONEY
C RANDOW
RDRLWMP E
S BARTUS